

# Signatures of linear Breit-Wheeler pair production in polarized $\gamma\gamma$ collisions

Qian Zhao,<sup>1</sup> Liang Tang,<sup>2</sup> Feng Wan,<sup>1</sup> Bo-Chao Liu,<sup>1</sup> Ruo-Yu Liu,<sup>3</sup> Rui-Zhi Yang,<sup>4</sup> Jin-Qing Yu,<sup>5,\*</sup> Xue-Guang Ren,<sup>1</sup> Zhong-Feng Xu,<sup>1</sup> Yong-Tao Zhao,<sup>1</sup> Yong-Sheng Huang,<sup>6,7,†</sup> and Jian-Xing Li<sup>1,‡</sup>

<sup>1</sup>*Ministry of Education Key Laboratory for Nonequilibrium Synthesis and Modulation of Condensed Matter, Shaanxi Province Key Laboratory of Quantum Information and Quantum Optoelectronic Devices, School of Physics, Xi'an Jiaotong University, Xi'an 710049, China*

<sup>2</sup>*College of Physics and Hebei Key Laboratory of Photophysics Research and Application, Hebei Normal University, Shijiazhuang 050024, China*

<sup>3</sup>*School of Astronomy and Space Science, Nanjing University, 210023 Nanjing, Jiangsu, China*

<sup>4</sup>*CAS Key Laboratory for Research in Galaxies and Cosmology, Department of Astronomy, School of Physical Sciences,*

*University of Science and Technology of China, Hefei, Anhui 230026, China*

<sup>5</sup>*School of Physics and Electronics, Hunan University, Changsha 410082, China*

<sup>6</sup>*School of Science, Shenzhen Campus of Sun Yat-sen University, Shenzhen 518107, P.R. China*

<sup>7</sup>*Institute of High Energy Physics, Chinese Academy of Sciences, Beijing 100049, China*

(Dated: November 30, 2021)

Laser-driven brilliant controllable polarized  $\gamma$ -photon sources open the way for designing compact  $\gamma\gamma$  collider, which enable the large yield of linear Breit-Wheeler (LBW) pairs in a single shot and thus provide an opportunity for the investigation of polarized LBW process. In this work we investigate the polarization characteristics of LBW pair production via our developed spin-resolved binary collision simulation method. Polarization of  $\gamma$ -photons modifies the kinematics of scattering particles and induces the correlated energy-angle shift of LBW pairs, and the latter's polarization characteristic depends on the helicity configurations of scattering particles. Our method confirms that the polarized  $\gamma\gamma$  collider with an asymmetric setup can be performed with currently achievable laser facilities to produce abundant polarized LBW pairs, fulfilling the detection power of polarimetries. The precise knowledge of polarized LBW process is in favor of the calibration and monitor of polarized  $\gamma\gamma$  collider, and could enhance the opacity of  $\gamma$ -photons in high-energy astrophysical objects to exacerbate the inconsistency between some observations and standard models.

Quantum electrodynamics (QED) predicts the interaction between two real photons, which leads to the linear Breit-Wheeler (LBW) electron-positron ( $e^\pm$ ) pair production [1] and photon-photon elastic scattering [2]. Although both the processes are observed in the collision of two virtual photons by means of the equivalent photon approximation of ultra-relativistic heavy-ion beams [3, 4], the validation via real photon-photon collisions has never been realized due to the lack of high-brilliance  $\gamma$ -photon beam. One of the most important physical projects in the planned  $\gamma\gamma$  collider is to search for higher-order photon-photon scattering, which is the solid evidence of the vacuum polarization and is of interest as a search for new physics [5–7]. Because the cross section of the lowest-order LBW process is several orders of magnitude larger than that of the photon-photon scattering [8], it produces useful signatures for diagnostics, feedback, and luminosity optimization in a  $\gamma\gamma$  collider [9, 10]. Therefore, it is necessary to investigate the comprehensive physics of the LBW process, especially with polarized photons and energy distribution. Moreover, despite the significance in validating basic QED theory, the LBW process is one of the most elemental ingredients of pair plasma production in high-energy astrophysical environment [11], such as  $\gamma$ -ray bursts [12], black hole accretion [13, 14] and active galactic nuclei [15].

Thanks to the developments of  $\gamma$ -photon sources driven by the electron beams of laser wakefield acceleration [16], high-brilliance  $\gamma$ -photon beams with MeV energy can be produced experimentally through bremsstrahlung [17, 18], nonlinear Thomson scattering [19, 20] and inverse Compton scattering [21–23], which open the way to investigate the real photon-photon interaction. Recently, numerous theoretical proposals on the  $\gamma\gamma$  collider are put forward to validate the LBW process [8, 24–32]. Among those proposals, the  $\gamma\gamma$  collider is designed either with GeV-energy photons from bremsstrahlung inside a high-Z target and keV-energy partner photon from laser-target radiation or X-ray free-electron laser [24, 30, 32], or with two same MeV  $\gamma$ -photon sources from laser-driven synchrotron or nonlinear Compton scattering [8, 25–27, 29]. Moreover, the dominated LBW process is studied in laser-driven plasmas [33, 34], and the quasiparticle-hole pair production in gapped graphene monolayers can be analogous to the LBW process [35]. However, above proposals mainly focus attention on the large pair yield, but generally ignore the inherent spin effects of scattering particles. The polarization transfer (i.e., helicity transfer) between initial photons and final  $e^\pm$  pairs is associated with their spin angular momentum. Based on the production of high-brilliance photons with highly circular polarization [36–41], the LBW process can be investigated in a polarized  $\gamma\gamma$  collider. The fundamental physics of helicity in the LBW process has been analyzed qualitatively from the perspective of angular momentum conservation [42]. The latest experiment confirms that the linearly polarized photons can induce the azimuthal-angle distribution of the LBW pairs [4], since the linear polarization is related to the azimuthal angle

\* jinqing.yu@hnu.edu.cn

† huangys59@mail.sysu.edu.cn

‡ jianxing@xjtu.edu.cn

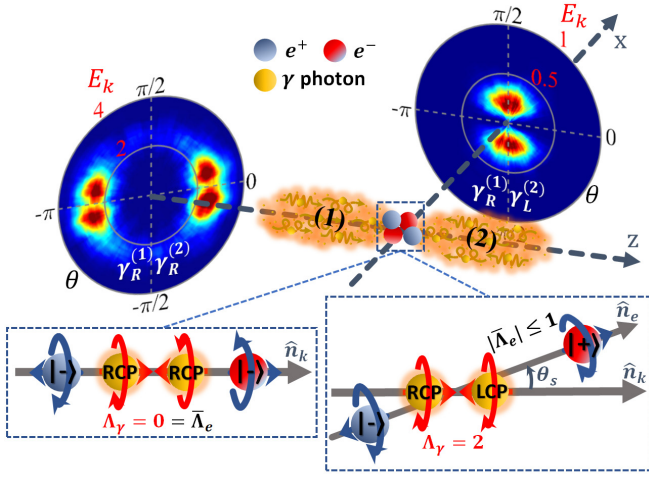


FIG. 1. Scenario of the LBW pair production in a colliding setup of polarized  $\gamma$ -photon beams in  $x-z$  plane in the laboratory frame. The pair spectra are presented in the plane of polar angle  $\theta$  and kinematic energy  $E_k$ . The lower sketches show the helicity transfer of the LBW process in the center of mass (c.m.) frame, and  $\Lambda_\gamma$  is the total helicity of two-photon system in the direction of photon momentum  $\hat{n}_k$ . The scattered pair carries the mean total helicity  $\bar{\Lambda}_e$  in the direction of electron momentum  $\hat{n}_e$ ,  $|\pm\rangle$  represent the positive and negative helicity states, corresponding to the right-hand and left-hand spirals, respectively, and  $\gamma_{R/L}^{(1/2)}$  denote right-hand circular polarization (RCP) or left-hand circular polarization (LCP) photon in beam (1) and beam (2), respectively.

of pair momenta. In addition, the impact of energy distribution of  $\gamma$ -photon beam on the LBW pair yield is analyzed in a semi-analytical model [31]. However, considering realistic polarization and energy distribution into laser-driven  $\gamma$ -photon beams, the spin-associated momentum and polarization characteristics of the LBW process have not been uncovered and are still great challenges.

In this Letter, we investigate the complete polarization effects in the LBW process by virtue of our first developed spin-resolved Monte Carlo (MC) simulation method, which is applicable for general binary collisions of leptons and photons (see the interaction scenario in Fig. 1). We find that the circular polarization of  $\gamma$ -photons can modify the kinematics of scattering particles and induces a correlated energy-angle shift of the LBW pairs (see the upper panel in Fig. 1 and more details in Fig. 2), and the polarization characteristic of the LBW pairs depends on the helicity configurations of scattering particles (see lower panel in Fig. 1 and more details in Fig. 3). Our method confirms that the polarized  $\gamma\gamma$  collider with an asymmetric setup can be performed with currently achievable laser facilities (see Tab. I), and the considered polarization effects may have significant applications in high-energy astrophysics.

Let us first summarize our simulation method for calculating the production and polarization of the LBW pairs. Employing the standard treatment of particle density matrixes in the scattering amplitude of incoherent binary collisions [42–47], the

polarized LBW cross section is obtained as

$$\frac{d\sigma}{d\Omega} = \sigma_0 \left[ F + \sum_{i=1}^3 (G_i^+ \zeta_i^+ + G_i^- \zeta_i^-) + \sum_{i,j=1}^3 H_{i,j} \zeta_i^+ \zeta_j^- \right], \quad (1)$$

where  $\sigma_0 = r_e^2 m_e^2 |\mathbf{p}_e| / 16\epsilon^3$ ,  $\Omega$  is the solid angle,  $\mathbf{p}_e$  the c.m. momentum of electron,  $\epsilon$  the c.m. energy of photon, electron and positron (they are equal in the c.m. frame),  $m_e$  and  $r_e$  the electron mass and classical radius, respectively,  $\zeta_i^\pm$  the spin components of electron (“−”) and positron (“+”), and the factors  $F$ ,  $G_i^\pm$  and  $H_{i,j}$  include the photon Stokes parameters  $\xi_i$  [43] and are given in [48]. Summing over  $\zeta_i^\pm$  and integrating over  $\Omega$ , one obtains

$$\begin{aligned} \bar{\sigma}_{tot} = & \frac{r_e^2 m_e^4 \pi}{4\epsilon^4} \sqrt{\frac{s-4}{s}} \left( -s-4 + 2\xi_1^{(1)} \xi_1^{(2)} + 3s\xi_2^{(1)} \xi_2^{(2)} \right. \\ & - 2\xi_3^{(1)} \xi_3^{(2)} \left. \right) + \frac{16\pi}{s} \tanh^{-1} \sqrt{\frac{s-4}{s}} (2s^2 + 8s - 16 \\ & + 8\xi_1^{(1)} \xi_1^{(2)} - 2s^2 \xi_2^{(1)} \xi_2^{(2)} - 8\xi_3^{(1)} \xi_3^{(2)}), \quad (2) \end{aligned}$$

where  $s = 4\epsilon^2/m_e^2$ . Relativistic units with  $c = \hbar = 1$  are used throughout.

The event probabilities are given by  $\bar{\sigma}_{tot}$  and the pair production is determined by a rejection method. The colliding photons in each 3-dimensional cell are paired in the laboratory frame using the no-time-counter method [49]. By Lorentz boost along the c.m. frame velocity  $\beta_{cm}$  [50–52], the 4-momenta of paired photons are transformed into the c.m. frame to calculate  $\mathbf{p}_e$ , which is determined by the probabilistic scattering angle  $\theta_s$ . Here  $\theta_s$  is calculated by solving  $\bar{\sigma}_\theta / \bar{\sigma}_{tot} = R_1 \in (-1, 1)$ , where  $R_1$  is a uniform random number and  $\bar{\sigma}_\theta = \sqrt{s(s-4)}/4 \int_{-|\cos\theta_s|}^{|\cos\theta_s|} d\bar{\sigma}$ . Moreover, the energy and momenta of  $e^\pm$  in the laboratory frame are obtained by the inverse Lorentz boost acting on  $\epsilon$  and  $\mathbf{p}_e$ .

The mean spin polarization vectors of electron and positron  $\bar{\zeta}^\pm$  are determined by the defined 3-vector basis [44, 48] and their components can be analytically calculated via  $\bar{\zeta}_i^\pm = G_i^\pm / F$  [43]. The corresponding mean helicities are  $\lambda_\pm = \mp \bar{\zeta}^\pm \mathbf{p}_e / 2|\mathbf{p}_e|$ . In our MC method, the projections of  $\bar{\zeta}^\pm$  onto the defined spin states  $\mathbf{D}^\pm$  (unit vectors) of a detector are calculated with transition probabilities, and the latter determine the sign of components  $D_i^\pm = \bar{\zeta}_i^\pm / |\bar{\zeta}^\pm|$ . Consequently, the total beam polarization is calculated by  $P_{tot} = \sqrt{(\bar{D}_1^\pm)^2 + (\bar{D}_2^\pm)^2 + (\bar{D}_3^\pm)^2}$ , where  $\bar{D}_i^\pm = \sum_{n=1}^N D_i^{\pm n} / N$  with the particle number  $N$  [53]. Aligning  $\mathbf{D}^\pm$  to the parallel or perpendicular direction of the momenta can further obtain the longitudinal polarization  $P_L$  or transverse polarization  $P_T$  for  $e^\pm$  beams. More details of our simulation method are clarified in the Supplementary Materials [48].

Impact of the  $\gamma$ -photon polarization on the energy and polar angle distributions of the LBW pairs is shown in Fig. 2.  $\bar{\sigma}_{tot}$  of the  $\gamma_R^{(1)} \gamma_R^{(2)}$  case increases about 33% at the peak energy and narrows the spectrum, compared with that of the nonpolarized case [see Fig. 2(a)], while the linear polarization only modifies the amplitude because it has no impact on  $\theta_s$  [48].

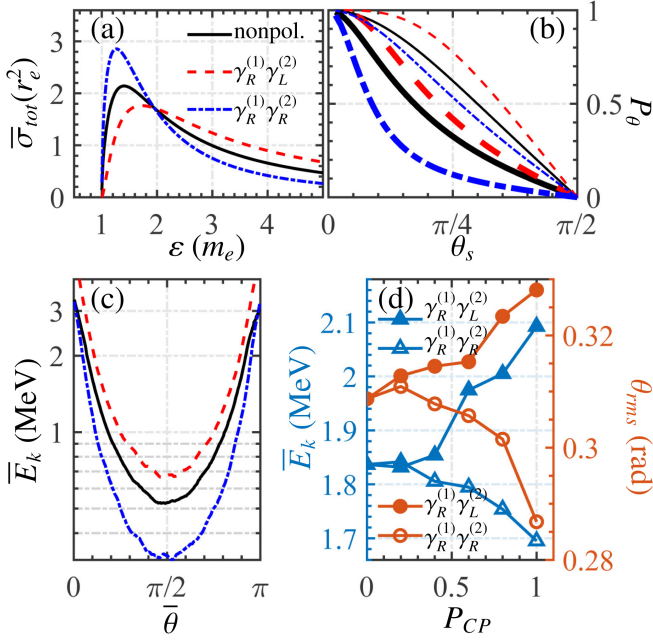


FIG. 2. (a)  $\bar{\sigma}_{tot}$  vs the c.m. energy  $\varepsilon$  for different collision schemes. The black-solid, red-dashed and blue-dash-dotted lines in (a) and (b) indicate the cases of employing nonpolarized,  $\gamma_R^{(1)}\gamma_L^{(2)}$  and  $\gamma_R^{(1)}\gamma_R^{(2)}$   $\gamma$ -photons, respectively. (b)  $P_\theta = \bar{\sigma}_\theta/\bar{\sigma}_{tot}$  vs  $\theta_s$ . The thin and thick lines correspond to  $\varepsilon = 1.4$  and 4, respectively. (c) Average kinetic energy  $\bar{E}_k$  vs average polar angle  $\bar{\theta}$  of positrons. (d)  $\bar{E}_k$  and divergence angle  $\theta_{rms}$  (root-mean-square deviation) of positrons beamed into  $0 < \theta < \pi/6$  vs average circular polarization  $P_{CP}$  of the initial  $\gamma$ -photon beam. The results in (c) and (d) are simulated with colliding  $\gamma$ -photon beams with an exponential energy distribution at an average energy 2 MeV and a divergence angle 0.1 rad in the laboratory frame.

A definite-shaped  $P_\theta(\theta_s)$  implies that the produced electron (positron) is scattered into a certain range of  $d\theta_s$  with a corresponding probability of  $dP_\theta$  [see Fig. 2(b)]. The reactions within  $\theta_s \lesssim \pi/6$  in the  $\gamma_R^{(1)}\gamma_L^{(2)}$  collision near threshold energy are almost forbidden due to the approximate zero probabilities, which lead to a dipole angular spectrum around the perpendicular direction of the colliding axis. By contrast, the dominated reactions occur within  $\theta_s \lesssim \pi/6$  in the  $\gamma_R^{(1)}\gamma_R^{(2)}$  collision at the energy much beyond the threshold, which lead to a quadrupole angular spectrum around the colliding axis (see energy-angle spectra Fig. 1). The distinct energy-correlated  $\theta_s$  in these two interaction schemes causes the energy-angle correlation of the pairs, whereby the  $\gamma_R^{(1)}\gamma_L^{(2)}$  collision results in the larger kinetic energy  $\bar{E}_k$  than that of the  $\gamma_R^{(1)}\gamma_R^{(2)}$  collision [see Fig. 2(c)]. As the initial circular polarization ( $P_{CP}$ ) of  $\gamma$ -photons increases, in the  $\gamma_R^{(1)}\gamma_L^{(2)}$  collision the average kinetic energy  $\bar{E}_k$  and the divergence angle  $\theta_{rms}$  of positrons both increase as well, while in the  $\gamma_R^{(1)}\gamma_R^{(2)}$  collision the tendency is inverse [see Fig. 2(d)]. Thus,  $\theta_{rms}$  is positively correlated to  $\bar{E}_k$ . The influence of the energy and divergence-angle fluctuations of the  $\gamma$ -photon beams on  $\theta_{rms}$  and  $\bar{E}_k$  is estimated in [48] and uniform results can be obtained with flexible parameters. Note that the correlated polar angle and energy distributions of the LBW pairs can be resolved precisely in experiments by the single particle

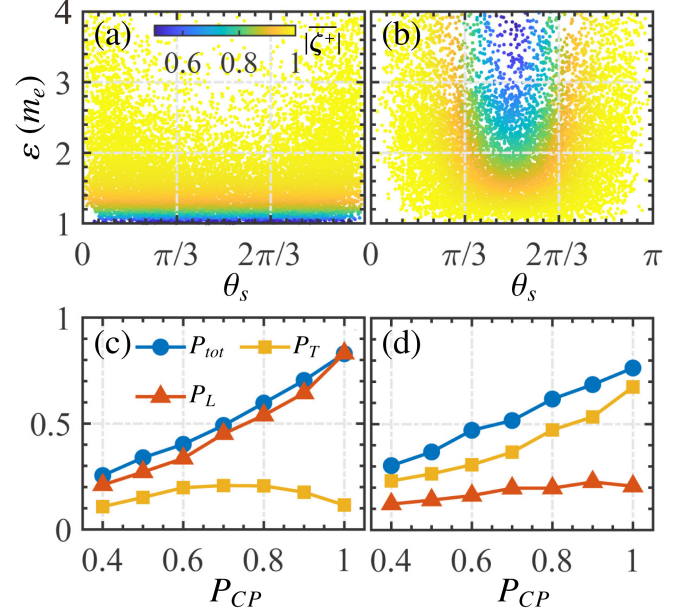


FIG. 3. (a) and (b): Distributions of  $|\zeta^+|$  of produced positrons for the  $\gamma_R^{(1)}\gamma_R^{(2)}$  and  $\gamma_R^{(1)}\gamma_L^{(2)}$  collisions, respectively. (c) and (d): Variations of  $P_{tot}$ ,  $P_L$  and  $P_T$  of positrons with respect to  $P_{CP}$  of the  $\gamma$ -photon beam, extracted from positrons within  $0 < \theta < \pi/6$  for the  $\gamma_R^{(1)}\gamma_R^{(2)}$  collision and  $\pi/3 < \theta < 2\pi/3$  for the  $\gamma_R^{(1)}\gamma_L^{(2)}$  collision, respectively. Here employed  $\gamma$ -photon beams both have an uniform energy distribution between 0.1 MeV and 2 MeV.

detector [32].

Particularly, the spin-polarization of the LBW pairs is derived from the circular polarization of parent  $\gamma$ -photons. For the  $\gamma_R^{(1)}\gamma_R^{(2)}$  collision, the partial polarization is produced near the threshold energy of the pair production [see Fig. 3(a)], while for the  $\gamma_R^{(1)}\gamma_L^{(2)}$  collision, the partial polarization is produced around  $\theta_s = \pi/2$  [see Fig. 3(b)]. It is nontrivial to reveal the variation of the positron polarization with respect to the  $\gamma$ -photon polarization. For the  $\gamma_R^{(1)}\gamma_R^{(2)}$  collision,  $P_L$  dominates the polarization and increases linearly, and  $P_T$  [attributed to the  $d\sigma_{+-\mp\mp}$  channel; see Fig. 4(e)] is less than 0.2 as  $P_{CP}$  varies [see Fig. 3(c)], since the produced pairs possess sole negative helicities [see Fig. 4(a)]. While, for the  $\gamma_R^{(1)}\gamma_L^{(2)}$  collision  $P_T$  dominates the polarization [see Fig. 3(d)], since the produced pairs possess the mixed helicity states [54] around  $\theta_s = \pi/2$  and the magnitude of  $P_T$  is affected by the extracted polar angle range [see Fig. 4(b)]. Thus, one could observe the signatures of polarization in the LBW process either via detecting  $P_L$  in the  $\gamma_R^{(1)}\gamma_R^{(2)}$  collision around the colliding axis or via detecting  $P_T$  in the  $\gamma_R^{(1)}\gamma_L^{(2)}$  collision around the perpendicular direction of the colliding axis.

The physical mechanism of the helicity transfer in the LBW process is analyzed in Fig. 4. The polarization is derived from the mean-helicity distribution, and the  $\gamma_R^{(1)}\gamma_R^{(2)}$  collision leads to the energy-dependent negative helicities, while the  $\gamma_R^{(1)}\gamma_L^{(2)}$  collision leads to the angle-dependent alternating helicities (vary between -0.5 and 0.5) [see Figs. 4(a) and (b)]. The positron helicity originates from the superposition of various helicity

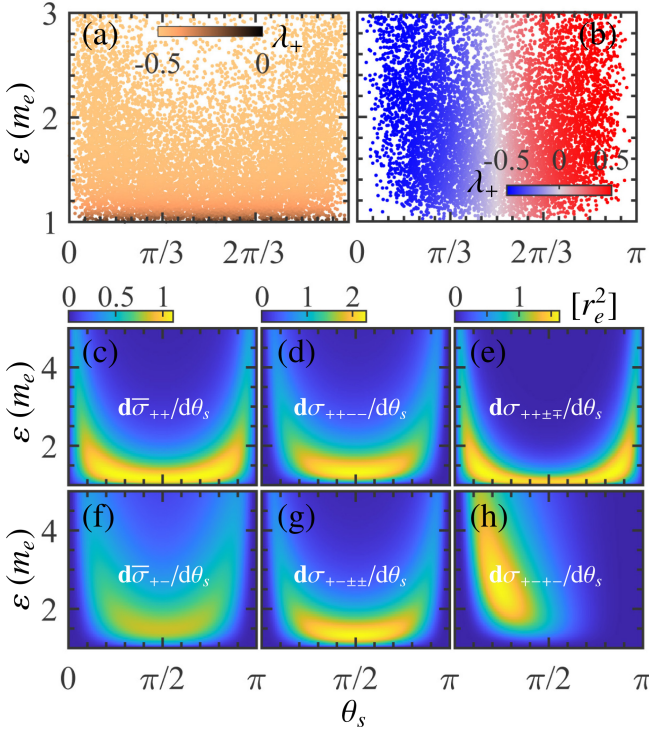


FIG. 4. (a) and (b): Distributions of the positron helicity  $\lambda_+$  with respect to  $\theta_s$  and  $\varepsilon$  in the c.m. frame for the  $\gamma_R^{(1)}\gamma_R^{(2)}$  and  $\gamma_R^{(1)}\gamma_L^{(2)}$  collisions, respectively. Employed parameters are the same with those in Fig. 3. (c)-(e) [(f)-(h)]: Differential cross sections for different helicity channels for the  $\gamma_R^{(1)}\gamma_R^{(2)}$  ( $\gamma_R^{(1)}\gamma_L^{(2)}$ ) collision. Here the subscripts from the first to the fourth in sequence denote positive (“+”) or negative (“-”) helicity eigenstates of  $\gamma^{(1)}$ ,  $\gamma^{(2)}$ ,  $e^-$ , and  $e^+$ , and  $d\bar{\sigma}$  indicates the spin-summarized cross section and is calculated via  $\sigma_0 F$  in Eq. (1).

eigenstates with different weights determined by the differential cross section. There are only three non-vanished helicity channels  $d\sigma_{+-+}$ ,  $d\sigma_{+++}$  and  $d\sigma_{++-}$  for the  $\gamma_R^{(1)}\gamma_R^{(2)}$  collision [see Figs. 4(d) and (e)]. Here,  $d\sigma_{+++}$  dominate the reaction near the threshold energy, produce the positrons at the helicity states  $|+\rangle$  or  $|-\rangle$  with the same weights, and consequently, cancel each other (i.e.,  $P_L$  vanishes and  $P_T$  maximizes). Thus, only the channel of  $d\sigma_{+-+}$  contributes to the state  $|-\rangle$ , i.e.,  $d\sigma_{+-+}$  solely induces  $P_L$ . These helicity channels finally result in the mean helicity distribution in Fig. 4(a) and the corresponding positron polarization in Fig. 3(a). Similarly, in the  $\gamma_R^{(1)}\gamma_L^{(2)}$  collision, there are four helicity channels  $d\sigma_{+--}$  and  $d\sigma_{+-+}$  (note that here  $d\sigma_{+--}$  is symmetric about  $\theta_s = \pi/2$  with  $d\sigma_{+-+}$  and thus is not shown) [see Figs. 4(g) and (h)].  $d\sigma_{+--}$  only contribute to  $P_T$  and  $d\sigma_{+-+}$  mainly to  $P_L$  [see Figs. 4(b) and 3(b)].

For the experimental feasibility, the symmetric and asymmetric setups are considered to design the polarized  $\gamma\gamma$  collider, as shown in Table I. The symmetric setup reveals the polarization-associated signatures in both of momentum and spin (see Figs. 2 and 3), and the required minimal brilliance of the  $\gamma$ -photon beam is rather high in order to produce a resolvable mA current for the polarimetry. In the asymmetric setup, the RCP  $\gamma$ -photon beam injects into a nonpolarized X-ray bath with a uniform

TABLE I. Average current  $I$  and polarization (Pol.) of produced positrons (electrons) extracted from the polar angle range of  $\Delta\theta$ . The symmetric setup includes photons number  $N_\gamma$ , brilliance  $\mathcal{B}_\gamma$  (photons  $s^{-1}mm^{-2}mrad^{-2}0.1\%BW$ ), and cross angle of colliding  $\gamma$ -photon beams. And the asymmetric setup considers a RCP  $\gamma$ -photon beam with 80% polarization colliding with a X-ray beam with uniform density  $n_X$ . Employed  $\gamma$ -photon beam in the symmetric (asymmetric) setup has a  $\sim 80$  fs duration and an exponential energy distribution averaged at 2 (100) MeV.

beam parameters	collisions	$I$ [mA]	Pol.	$\Delta\theta$ [rad]
Symmetric Setup: $N_\gamma : 1 \times 10^{11}$ Photons.	$\gamma_R^{(1)}\gamma_R^{(2)}$	4.231	$P_L$	$0 \pm \pi/6$
$\mathcal{B}_\gamma : 1.5 \times 10^{23}$ cross-angle: $5^\circ$	$\gamma_R^{(1)}\gamma_L^{(2)}$	3.952	$P_T$	$\pi/2 \pm \pi/6$
Asymmetric Setup: $N_\gamma : 1 \times 10^7$ Photons.	$\gamma_R^{(1)}(0.8)$	1.052	$P_L(0.348)$ ,	$0 \pm 0.02$
$\mathcal{B}_\gamma : 2.2 \times 10^{21}$ $n_X : 9.3 \times 10^{23} cm^{-3}$	X-ray		$P_T(0.151)$	

energy distribution between 1 – 3 keV [32], produce a strongly collimated positron (electron) beam with moderate  $P_L$  and  $P_T$ . This asymmetric setup significantly reduces the required minimal brilliance of the  $\gamma$ -photon beam which is experimentally feasible through inverse Compton scattering [21, 55], and the polarized one is also available by bremsstrahlung radiation with  $\sim 10^8$  photons [24, 39, 40]. The yield and polarization stabilities are estimated when the divergence angle and the polarization of the  $\gamma$ -photon beam change and uniform results are obtained (see [48]). In terms of the polarization detection, the  $e^\pm$  polarimetry technology has achieved a high precision  $\leq 1\%$ , e.g., Compton transmission polarimetry [37–39] and Mott polarimetry [56–58], which are both applicable at the energy of 0.1 – 10 MeV and can response the current as low as  $\leq 100\mu A$  [56, 57].

Furthermore, we underline that the LBW process is widely involved in high-energy astrophysical phenomena. The measured  $\gamma$ -ray spectra of those intense compact astrophysical objects (such as GRBs, blazars, and etc) are supposed to be attenuated at the high-energy end by the low-energy radiation therein via this process [59–62]. Both the low-energy radiation and the  $\gamma$ -ray radiation, which generally arise from the synchrotron radiation and the inverse Compton scattering respectively, can be polarized in the presence of magnetic field. Taking into account the polarized LBW process would enhance the opacity of  $\gamma$ -photons of those sources and consequently exacerbate the inconsistency between some observations and standard models, which may challenge the current understanding on the astrophysical objects. One example is the discovery of minute-scale  $\gamma$ -ray variability in many blazars [e.g. 63–65]. The fast variability implies a compact radiation zone so that an unrealistically large Doppler factor with  $\delta_D > 50$  has to be invoked in order to avoid significant attenuation of the  $\gamma$ -ray flux [66], under the current standard picture of the blazar’s jet. The value is significantly larger than the Doppler factors inferred from superluminal motions of blazar jets as revealed

by radio observations, which is typically around 10 [67]. This is referred to as the “Doppler factor crisis” [15] and has important implications for the internal structure of the blazar jet [68], the external gaseous environment [69] or the acceleration mechanism of the relativistic outflow driven by supermassive black hole [70]. Besides, considering the polarized LBW process could be quite helpful to reveal the radiation mechanism of a pulsar, since the density distribution of the pair plasma in the magnetosphere of a pulsar is distorted by the polarized effect [71].

In conclusion, we develop a fully spin-resolved simulation method for general binary collisions to investigate the complete polarization effects of the LBW process in polarized  $\gamma\gamma$  collision. Qualitative signatures of polarized LBW process are imprinted on momentum and spin of produced pairs. The precise physics of polarized LBW process is effective to calibrate and monitor the upcoming polarized  $\gamma\gamma$  collider,

and paves the way for proceeding the elusive photon-photon scattering. Besides, the polarization-induced fluctuations of the  $e^\pm$  density in high-energy astrophysical objects possibly associate with certain of significant observations, which calls for the further investigation.

*Acknowledgement:* This work is supported by the National Natural Science Foundation of China (Grants Nos. 12022506, 11874295, 11875219, 11905169, 12175058), the China Postdoctoral Science Foundation (Grant No. 2020M683447), the Natural Science Foundation of Hunan Province, China (Grant No. 2020JJ5031), the project of Science and Technology on plasma physics Laboratory (No. 6142A04190111), the Innovation Project of IHEP (542017IHEPZZBS11820, 542018IHEPZZBS12427), and the CAS Center for Excellence in Particle Physics (CCEPP).

- 
- [1] G. Breit and J. A. Wheeler, Collision of two light quanta, *Phys. Rev.* **46**, 1087 (1934).
- [2] O. Halpern, Scattering processes produced by electrons in negative energy states, *Phys. Rev.* **44**, 855 (1933).
- [3] ATLAS Collaboration, Evidence for light-by-light scattering in heavy-ion collisions with the ATLAS detector at the LHC, *Nat. Phys.* **13**, 852 (2017).
- [4] J. Adam, L. Adamczyk, J. Adams, J. Adkins, G. Agakishiev, M. M. Aggarwal, Z. Ahammed, I. Alekseev, D. Anderson, A. Aparin, *et al.* (STAR Collaboration), Measurement of  $e^+e^-$  momentum and angular distributions from linearly polarized photon collisions, *Phys. Rev. Lett.* **127**, 052302 (2021).
- [5] T. Yamaji, T. Inada, T. Yamazaki, T. Namba, S. Asai, T. Kobayashi, K. Tamasaku, Y. Tanaka, Y. Inubushi, K. Sawada, M. Yabashi, and T. Ishikawa, An experiment of X-ray photon-photon elastic scattering with a Laue-case beam collider, *Phys. Lett. B* **763**, 454 (2016).
- [6] I. Drebot, A. Bacci, D. Micieli, E. Milotti, V. Petrillo, M. R. Conti, A. R. Rossi, E. Tassi, and L. Serafini, Study of photon-photon scattering events, *Nucl. Instrum. Methods Phys. Res., Sect. A* **865**, 9 (2017).
- [7] T. Takahashi, G. An, Y. Chen, W. Chou, Y. Huang, W. Liu, W. Lu, J. Lv, G. Pei, S. Pei, C. P. Shen, B. Sun, C. Zhang, and C. Zhang, Light-by-Light scattering in a photon-photon collider, *Eur. Phys. J. C* **78**, 893 (2018).
- [8] I. Drebot, D. Micieli, E. Milotti, V. Petrillo, E. Tassi, and L. Serafini, Matter from light-light scattering via Breit-Wheeler events produced by two interacting Compton sources, *Phys. Rev. Accel. Beams* **20**, 043402 (2017).
- [9] A. V. Pak, D. V. Pavluchenko, S. S. Petrosyan, V. G. Serbo, and V. I. Telnov, Measurement of  $\gamma\gamma$  and  $\gamma e$  luminosities and polarizations at photon colliders, *Nucl. Phys. B-Proc. Suppl.* **126**, 379 (2004).
- [10] J. Esberg, U. I. Uggerhøj, B. Dalena, and D. Schulte, Strong field processes in beam-beam interactions at the compact linear collider, *Phys. Rev. ST Accel. Beams* **17**, 051003 (2014).
- [11] R. Ruffini, G. Vereshchagin, and S. Xue, Electron-positron pairs in physics and astrophysics: From heavy nuclei to black holes, *Phys. Rep.* **487**, 1 (2010).
- [12] P. Kumar and B. Zhang, The physics of gamma-ray bursts relativistic jets, *Phys. Rep.* **561**, 1 (2015).
- [13] K. Hirotani and H. Y. Pu, Energetic gamma radiation from rapidly rotating black holes, *Astrophys. J.* **818**, 50 (2016).
- [14] K. Akiyama, A. Alberdi, W. Alef, K. Asada, R. Azulay, A. K. Baccko, D. Ball, M. Baloković, J. Barrett, D. Bintley, *et al.*, First M87 event horizon telescope results. v. physical origin of the asymmetric ring, *Astrophys. J. Lett.* **875**, L5 (2019).
- [15] M. Böttcher, Progress in multi-wavelength and multi-messenger observations of blazars and theoretical challenges, *Galaxies* **7**, 20 (2019).
- [16] E. Esarey, C. B. Schroeder, and W. P. Leemans, Physics of laser-driven plasma-based electron accelerators, *Rev. Mod. Phys.* **81**, 1229 (2009).
- [17] Y. Glinec, J. Faure, L. LeDain, S. Darbon, T. Hosokai, J. J. Santos, E. Lefebvre, J. P. Rousseau, F. Burgy, B. Mercier, and V. Malka, High-resolution  $\gamma$ -ray radiography produced by a laser-plasma driven electron source, *Phys. Rev. Lett.* **94**, 025003 (2005).
- [18] N. Lemos, F. Albert, J. L. Shaw, D. Papp, R. Polanek, P. King, A. L. Milder, K. A. Marsh, A. Pak, B. B. Pollock, *et al.*, Bremsstrahlung hard X-ray source driven by an electron beam from a self-modulated laser wakefield accelerator, *Plasma Phys. Control. Fusion* **60**, 054008 (2018).
- [19] G. Sarri, D. J. Corvan, W. Schumaker, J. M. Cole, A. Di Piazza, H. Ahmed, C. Harvey, C. H. Keitel, K. Krushelnick, S. P. D. Mangles, Z. Najmudin, D. Symes, A. G. R. Thomas, M. Yeung, Z. Zhao, and M. Zepf, Ultrahigh brilliance multi-meV  $\gamma$ -ray beams from nonlinear relativistic thomson scattering, *Phys. Rev. Lett.* **113**, 224801 (2014).
- [20] W. Yan, C. Fruhling, G. Golovin, D. Haden, J. Luo, P. Zhang, B. Zhao, J. Zhang, C. Liu, M. Chen, S. Chen, S. Banerjee, and D. Umstadter, High-order multiphoton thomson scattering, *Nat. Photonics* **11**, 514 (2017).
- [21] C. Yu, R. Qi, W. Wang, J. Liu, W. Li, C. Wang, Z. Zhang, J. Liu, Z. Qin, M. Fang, *et al.*, Ultrahigh brilliance quasi-monochromatic MeV gamma-rays based on self-synchronized all-optical compton scattering, *Sci. Rep.* **6**, 29518 (2016).
- [22] J. M. Cole, K. T. Behm, E. Gerstmayr, T. G. Blackburn, J. C. Wood, C. D. Baird, M. J. Duff, C. Harvey, A. Ilderton, A. S. Joglekar, K. Krushelnick, S. Kuschel, M. Marklund, P. McKenna, C. D. Murphy, K. Poder, C. P. Ridgers, G. M. Samarin, G. Sarri, D. R. Symes, A. G. R. Thomas, J. Warwick, M. Zepf, Z. Naj-

- udin, and S. P. D. Mangles, Experimental evidence of radiation reaction in the collision of a high-intensity laser pulse with a laser-wakefield accelerated electron beam, *Phys. Rev. X* **8**, 011020 (2018).
- [23] X. L. Zhu, M. Chen, S. M. Weng, T. P. Yu, W. M. Wang, F. He, Z. M. Sheng, P. McKenna, D. A. Jaroszynski, and J. Zhang, Extremely brilliant GeV  $\gamma$ -rays from a two-stage laser-plasma accelerator, *Sci. Adv.* **6**, eaaz7240 (2020).
- [24] O. J. Pike, F. Mackenroth, E. G. Hill, and S. J. Rose, A photon-photon collider in a vacuum hohlraum, *Nat. Photonics* **8**, 434 (2014).
- [25] X. Ribeyre, E. d’Humières, O. Jansen, S. Jequier, V. T. Tikhonchuk, and M. Lobet, Pair creation in collision of gamma-ray beams produced with high-intensity lasers, *Phys. Rev. E* **93**, 013201 (2016).
- [26] O. Jansen, T. Wang, D. J. Stark, E. d’Humières, T. Toncian, and A. V. Arefiev, Leveraging extreme laser-driven magnetic fields for gamma-ray generation and pair production, *Plasma Phys. Control. Fusion* **60**, 054006 (2018).
- [27] J. Q. Yu, H. Y. Lu, T. Takahashi, R. H. Hu, Z. Gong, W. J. Ma, Y. S. Huang, C. E. Chen, and X. Q. Yan, Creation of electron-positron pairs in photon-photon collisions driven by 10-PW laser pulses, *Phys. Rev. Lett.* **122**, 014802 (2019).
- [28] T. Wang and A. Arefiev, Comment on “creation of electron-positron pairs in photon-photon collisions driven by 10-PW laser pulses”, *Phys. Rev. Lett.* **125**, 079501 (2020).
- [29] T. Wang, X. Ribeyre, Z. Gong, O. Jansen, E. d’Humières, D. Stutman, T. Toncian, and A. Arefiev, Power scaling for collimated  $\gamma$ -ray beams generated by structured laser-irradiated targets and its application to two-photon pair production, *Phys. Rev. Applied* **13**, 054024 (2020).
- [30] A. Golub, S. Villalba-Chávez, H. Ruhl, and C. Müller, Linear Breit-Wheeler pair production by high-energy bremsstrahlung photons colliding with an intense X-ray laser pulse, *Phys. Rev. D* **103**, 016009 (2021).
- [31] L. Esnault, E. d’Humières, A. Arefiev, and X. Ribeyre, Electron-positron pair production in the collision of real photon beams with wide energy distributions, arXiv:2103.09099.
- [32] B. Kettle, D. Hollatz, E. Gerstmayr, G. M. Samarin, A. Alejo, S. Astbury, C. D. Baird, S. Bohlen, M. Campbell, C. Colgan, *et al.*, A laser-plasma platform for photon-photon physics: the two photon Breit-Wheeler process, *New J. Phys.* **23**, 115006 (2021).
- [33] Y. He, T. G. Blackburn, T. Toncian, and A. V. Arefiev, Dominance of gamma-gamma electron-positron pair creation in a plasma driven by high-intensity lasers, *Commun. Phys.* **4**, 139 (2021).
- [34] Y. He, I. L. Yeh, T. G. Blackburn, and A. Arefiev, A single-laser scheme for observation of linear Breit-Wheeler electron-positron pair creation, *New J. Phys.* **23**, 115005 (2021).
- [35] A. Golub, R. Egger, C. Müller, and S. Villalba-Chávez, Dimensionality-driven photoproduction of massive Dirac pairs near threshold in gapped graphene monolayers, *Physical review letters* **124**, 110403 (2020).
- [36] V. Yakimenko and I. V. Pogorelsky, Polarized  $\gamma$  source based on compton backscattering in a laser cavity, *Phys. Rev. Spec. Top.-Accel. Beams* **9**, 091001 (2006).
- [37] T. Omori, M. Fukuda, T. Hirose, Y. Kurihara, R. Kuroda, M. Nomura, A. Ohashi, T. Okugi, K. Sakaue, T. Saito, J. Urakawa, M. Washio, and I. Yamazaki, Efficient propagation of polarization from laser photons to positrons through compton scattering and electron-positron pair creation, *Phys. Rev. Lett.* **96**, 114801 (2006).
- [38] G. Alexander, J. Barley, Y. Batygin, S. Berridge, V. Bharadwaj, G. Bower, W. Bugg, F.-J. Decker, R. Dollan, Y. Efremenko, V. Gharibyan, C. Hast, R. Iverson, H. Kolanoski, J. Kovermann, K. Laihem, T. Lohse, K. T. McDonald, A. A. Mikhailichenko, G. A. Moortgat-Pick, P. Pahl, R. Pitthan, R. Pöschl, E. Reinherz-Aronis, S. Riemann, A. Schälicke, K. P. Schüller, T. Schweizer, D. Scott, J. C. Sheppard, A. Stahl, Z. M. Szalata, D. Walz, and A. W. Weidemann, Observation of polarized positrons from an undulator-based source, *Phys. Rev. Lett.* **100**, 210801 (2008).
- [39] D. Abbott, P. Adderley, A. Adeyemi, P. Aguilera, M. Ali, H. Areti, M. Baylac, J. Benesch, G. Bosson, B. Cade, *et al.*, Production of highly polarized positrons using polarized electrons at MeV energies, *Phys. Rev. Lett.* **116**, 214801 (2016).
- [40] J. Yan, J. M. Mueller, M. W. Ahmed, H. Hao, S. Huang, J. Li, V. N. Litvinenko, P. Liu, S. F. Mikhailov, V. G. Popov, *et al.*, Precision control of gamma-ray polarization using a crossed helical undulator free-electron laser, *Nat. Photonics* **13**, 629 (2019).
- [41] Y. F. Li, R. Shaisultanov, Y. Y. Chen, F. Wan, K. Z. Hatsagortsyan, C. H. Keitel, and J. X. Li, Polarized ultrashort brilliant multi-GeV  $\gamma$  rays via single-shot laser-electron interaction, *Phys. Rev. Lett.* **124**, 014801 (2020).
- [42] A. G. Baier, V. N. Grozin, Complete analysis of polarization effects in  $\gamma\gamma \rightarrow e^+e^-$  with REDUCE, arXiv:0209361.
- [43] V. B. Berestetskii, E. M. Lifshitz, and L. P. Pitaevskii, *Quantum Electrodynamics*, Vol. 4 (Butterworth-Heinemann, 1982).
- [44] S. I. Kotkin, G. L. Polityko and V. G. Serbo, Polarization of final electrons in the compton effect, *Nucl. Instrum. Methods Phys. Res., Sect. A* **405**, 30 (1998).
- [45] A. G. Grozin, Complete analysis of polarization effects in  $e\gamma \rightarrow e\gamma$  with REDUCE, arXiv:0209360.
- [46] D. Y. Ivanov, G. L. Kotkin, and V. G. Serbo, Complete description of polarization effects in emission of a photon by an electron in the field of a strong laser wave, *Eur. Phys. J. C* **36**, 127 (2004).
- [47] D. Y. Ivanov, G. L. Kotkin, and V. G. Serbo, Complete description of polarization effects in  $e^+e^-$  pair production by a photon in the field of a strong laser wave, *Eur. Phys. J. C* **40** (2005).
- [48] Supplemental Materials mainly include the calculation of polarized LBW cross-section, the prescription of photon Stokes parameters and pair spin vectors, and the additional simulation results for polarized LBW pair production.
- [49] F. Del Gaudio, T. Grismayer, R. A. Fonseca, and L. O. Silva, Compton scattering in particle-in-cell codes, *J. Plasma Phys.* **86**, 905860516 (2020).
- [50] M. Schlickeiser and R. Bottcher, The pair production spectrum from photon-photon annihilation, *Astron. Astrophys.* **325**, 866 (1997).
- [51] X. Ribeyre, E. d’Humières, O. Jansen, S. Jequier, and V. T. Tikhonchuk, Electron-positron pairs beaming in the Breit-Wheeler process, *Plasma Phys. Control. Fusion* **59**, 014024 (2017).
- [52] X. Ribeyre, E. d’Humières, S. Jequier, and V. T. Tikhonchuk, Effect of differential cross section in Breit-Wheeler pair production, *Plasma Phys. Control. Fusion* **60**, 104001 (2018).
- [53] H. A. Tolhoek, Electron polarization, theory and experiment, *Rev. Mod. Phys.* **28**, 277 (1956).
- [54] K.-i. Hikasa, Transverse-polarization effects in  $e^+e^-$  collisions: The role of chiral symmetry, *Phys. Rev. D* **33**, 3203 (1986).
- [55] F. Albert, S. G. Anderson, D. J. Gibson, C. A. Hagmann, M. S. Johnson, M. Messerly, V. Semenov, M. Y. Shverdin, B. Rusnak, A. M. Tremaine, F. V. Hartemann, C. W. Siders, D. P. McNabb, and C. P. J. Barty, Characterization and applications of a tunable, laser-based, MeV-class compton-scattering  $\gamma$ -ray source, *Phys. Rev. Spec. Top.-Accel. Beams* **13**, 070704 (2010).
- [56] V. Tioukine, K. Aulenbacher, and E. Riehn, A mott polarimeter

- operating at MeV electron beam energies, *Rev. Sci. Instrum.* **82**, 033303 (2011).
- [57] K. Aulenbacher, E. Chudakov, D. Gaskell, J. Grames, and K. D. Paschke, Precision electron beam polarimetry for next generation nuclear physics experiments, *Int. J. Mod. Phys. E* **27**, 1830004 (2018).
- [58] J. M. Grames, C. K. Sinclair, M. Poelker, X. Roca-Maza, M. L. Stutzman, R. Suleiman, M. A. Mamun, M. McHugh, D. Moser, J. Hansknecht, B. Moffit, and T. J. Gay, High precision 5 MeV Mott polarimeter, *Phys. Rev. C* **102**, 015501 (2020).
- [59] J. Granot, J. Cohen-Tanugi, and E. d. C. e Silva, Opacity buildup in impulsive relativistic sources, *Astrophys. J.* **677**, 92 (2008).
- [60] D. Guetta, E. Pian, and E. Waxman, FERMI constraints on the high energy,  $\sim 1$  GeV, emission of long gamma ray bursts, *Astron. Astrophys.* **525**, A53 (2011).
- [61] J. Poutanen and B. Stern, GeV breaks in blazars as a result of gamma-ray absorption within the broad-line region, *Astrophys. J. Lett.* **717**, L118 (2010).
- [62] R. Xue, R. Y. Liu, X. Y. Wang, H. Yan, and M. Böttcher, On the minimum jet power of TeV BL lac objects in the  $p\text{-}\gamma$  model, *Astrophys. J.* **871**, 81 (2019).
- [63] F. Aharonian, A. Akhperjanian, A. R. Bazer-Bachi, B. Behera, M. Beilicke, W. Benbow, D. Berge, K. Bernlöhr, C. Boisson, O. Bolz, *et al.*, An exceptional very high energy gamma-ray flare of PKS 2155–304, *Astrophys. J. Lett.* **664**, L71 (2007).
- [64] T. Arlen, T. Aune, M. Beilicke, W. Benbow, A. Bouvier, J. H. Buckley, V. Bugaev, A. Cesarini, L. Ciupik, M. P. Connolly, *et al.*, Rapid TeV gamma-ray flaring of BL lacertae, *Astrophys. J.* **762**, 92 (2012).
- [65] M. Meyer, J. D. Scargle, and R. D. Blandford, Characterizing the gamma-ray variability of the brightest flat spectrum radio quasars observed with the fermi LAT, *Astrophys. J.* **877**, 39 (2019).
- [66] M. C. Begelman, A. C. Fabian, and M. J. Rees, Implications of very rapid TeV variability in blazars, *Mon. Not. Roy. Astron. Soc.* **384**, L19 (2008).
- [67] T. Hovatta, E. Valtaoja, M. Tornikoski, and A. Lähteenmäki, Doppler factors, lorentz factors and viewing angles for quasars, bl lacertae objects and radio galaxies, *Astron. Astrophys.* **494**, 527 (2009).
- [68] D. Giannios, D. A. Uzdensky, and M. C. Begelman, Fast TeV variability in blazars: jets in a jet, *Mon. Not. Roy. Astron. Soc.* **395**, L29 (2009).
- [69] M. Tavani, V. Vittorini, and A. Cavaliere, An emerging class of gamma-ray flares from blazars: Beyond one-zone models, *Astrophys. J.* **814**, 51 (2015).
- [70] M. Lyutikov and M. Lister, Resolving doppler-factor crisis in active galactic nuclei: Non-steady magnetized outflows, *Astrophys. J.* **722**, 197 (2010).
- [71] Y. S. Huang, Quantum-electrodynamical birefringence vanishing in a thermal relativistic pair plasma, *Sci. Rep.* **5**, 1 (2015).